

The effects of a magnetic field on planetary migration in laminar and turbulent discs

Megan L. Comins^{1*}, Marina M. Romanova¹, Alexander V. Koldoba^{2,3}, Galina V. Ustyugova⁴, Richard V.E. Lovelace^{1,5}

¹Department of Astronomy, Cornell University, Ithaca, NY 14853-6801

²Institute of Computer Aided Design RAS, 2nd Brestskaya st., 19/18, Moscow, 123056, Russia

³Moscow Institute of Physics and Technology, Dolgoprudny, Moscow Region, 141700, Russia

⁴Keldysh Institute for Applied Mathematics, Moscow, Russia

⁵Department of Applied and Engineering Physics, Cornell University, Ithaca, NY 14853-680

11 November 2021

ABSTRACT

We investigate the migration of low-mass planets ($5M_{\oplus}$ and $20M_{\oplus}$) in accretion discs threaded with a magnetic field using 2D MHD code in polar coordinates. We observed that, in the case of a strong azimuthal magnetic field where the plasma parameter is $\beta \sim 1-2$, density waves at the magnetic resonances exert a positive torque on the planet and may slow down or reverse its migration. However, when the magnetic field is weaker (i.e., the plasma parameter β is relatively large), then non-axisymmetric density waves excited by the planet lead to growth of the radial component of the field and, subsequently, to development of the magneto-rotational instability, such that the disc becomes turbulent. Migration in a turbulent disc is stochastic, and the migration direction may change as such. To understand migration in a turbulent disc, both the interaction between a planet and individual turbulent cells, as well as the interaction between a planet and ordered density waves, have been investigated.

Key words: accretion, accretion discs — magnetic fields — MHD — waves — planets and satellites: dynamical evolution and stability — planet-disc interactions

1 INTRODUCTION

The migration of protoplanets embedded in accretion discs has been extensively studied in recent years (see, e.g., review by Kley & Nelson 2012). A low-mass protoplanet excites density waves in the disc at the Lindblad resonances and migrates toward the star if no other torques are exerted (e.g., Goldreich & Tremaine 1979). However, a corotation torque originating near the planet can slow or even reverse the migration (e.g., Tanaka et al. 2002; Masset 2002; Masset et al. 2006). Another possible cause of slowed or reversed migration is the excitation of magnetic resonances in the disc when a relatively strong ($\beta \sim 1^1$) azimuthal magnetic field is present (Terquem 2003). These magnetic resonances can halt or reverse the migration of the planet if the magnetic field is sufficiently strong and it has a steep gradient toward the star. The action of this mechanism has been shown in numerical simulations by Fromang et al. (2005).

On the other hand, accretion discs threaded with a weak magnetic field are prone to the magneto-rotational instability (MRI; Balbus & Hawley 1991, 1998). Numerical simulations of planet migration in a turbulent disc have shown that the semimajor axis of the planet changes stochastically due to the planet's interaction with the turbulent cells in the disc. The migration rate can increase or decrease, and the direction of the migration can reverse (Nelson & Papaloizou 2004).

An initial goal of this paper was to more deeply investigate the effect of magnetic resonances on the migration of a low-mass embedded planet following the methods used by Fromang et al. (2005), albeit that we explored a larger parameter space with regards to the mass of the planet and the density distribution in the disc, as well as the magnetic field strength and its distribution in the disc. While exploring this expanded parameter space, we noticed the development of MRI-driven turbulence in the disc in many cases. In particular, when the magnetic field is weak, non-axisymmetric density waves excited by the planet lead to perturbations in the initially-azimuthal magnetic field and, subsequently, to growth of the radial component of the magnetic field near the planet. The azimuthal field grows with time due to the

* E-mail of corresponding author: mcomins@astro.cornell.edu

¹ $\beta = 8\pi P/B^2$, where P and B are the pressure and magnetic field in the disc, respectively

stretching of the radial field lines by the differential rotation of the Keplerian disc. As a result, an MRI-type instability develops and propagates to larger distances from the planet, and the disc becomes turbulent. The planet interacts with the turbulent cells, and the torque associated with this interaction is much larger than the torque seen prior to the development of turbulence (i.e., the torque due to magnetic resonances). Therefore, we also studied the parameter space describing the transition from a laminar to a turbulent disc, as well as the migration of a planet in a turbulent disc in detail.

We first describe how the migration rate and direction of a low-mass planet are affected by the planet mass, as well as the distribution of surface density and magnetic field in the laminar disc. We also show how these parameters alter the time at which the onset of turbulence occurs in magnetized discs. Finally, to better understand the interaction between the planet and turbulent cells in the disc, we study the torque on the planet by (1) an ordered, low-amplitude density wave generated at the inner boundary and (2) a high-amplitude wave that is excited in a turbulent MHD disc.

The plan for this paper is as follows. In §2 we overview the theory of the different sources of torque on the planet. In §3 we describe our physical model and numerical setup. In §4 we describe our main parameters. We describe our test simulations in the hydrodynamical disc in §5 and simulations in a laminar magnetic disc in §6. Migration in turbulent discs is shown in §7, and migration under the influence of density waves is shown in §8. We conclude in §9.

2 THEORETICAL BACKGROUND

In this section, we discuss the causes of inward and outward migration in hydrodynamic and MHD discs.

2.1 Migration in hydrodynamic discs

In the absence of a magnetic field in the disc, the migration of the planet is determined by the Lindblad and corotation torques (Goldreich & Tremaine 1979; Ward 1986, 1997). The Lindblad torque is generated when the planet excites m -armed waves in the disc with “orbital” frequencies $\omega = m\Omega_p$. The dispersion relation for these waves in a low-temperature, low-mass disc is $(\omega - m\Omega)^2 = \kappa^2$, where $\kappa = \Omega_{\text{Kep}}$ is the epicyclic frequency in a Keplerian disc. Substituting $\Omega(r) = \sqrt{GM_\star/r^3}$, the locations of the Lindblad resonances are

$$r_{\text{LR}} = r_p \left(\frac{m \pm 1}{m} \right)^{2/3}. \quad (1)$$

For each value of m (except $m = 1$), there is one resonance located closer to (farther from) the star than the planet called the inner (outer) Lindblad resonance. The inner Lindblad resonances exert a positive torque on the planet and “push” the planet outward, while the outer Lindblad resonances have the opposite effect. The total Lindblad torque (also known as the “differential Lindblad torque”) determines the migration direction in the absence of other torques. The differential Lindblad torque is negative, resulting in overall inward migration of the planet if there are no other sources of torque.

However, there is typically a corotation torque exerted on the planet as well. The physics of the corotation torque and

its effect on planet migration has been studied by number of authors (e.g., Paardekooper & Mellema 2006; Baruteau & Masset 2008; Paardekooper & Papaloizou 2008; Kley et al. 2009; Masset & Casoli 2009, 2010; Paardekooper et al. 2010, 2011). In an isothermal disc, both the magnitude and sign of the corotation torque depend on the gradient of the surface density at the corotation radius.

2.2 Migration in magnetized discs

2.2.1 Migration in laminar MHD discs due to magnetic resonances

In strongly magnetized laminar discs, magnetic waves can be excited, and torques associated with the magnetic waves can affect a planet’s migration. (e.g., Terquem 2003; Fromang et al. 2005; Fu & Lai 2011). Terquem (2003) investigated the propagation of waves in a magnetized disc in which the magnetic field is purely azimuthal and found that there are two singular radii at which the frequency perturbation in a frame rotating with the fluid matches that of a slow MHD wave propagating along the field lines; these radii define the locations of the magnetic resonances. The inner and outer magnetic resonances are denoted similarly to Lindblad resonances, with the inner magnetic resonances $r_{\text{IMR}} < r_p$, and the outer magnetic resonances $r_{\text{OMR}} > r_p$. Terquem (2003) derived the following dispersion relation:

$$m^2(\Omega - \Omega_p)^2 = \frac{m^2 c_s^2 v_A^2}{r^2(v_A^2 + c_s^2)}. \quad (2)$$

Here, v_A is the Alfvén speed, given by Terquem (2003) as $v_A^2 = \langle B^2 \rangle / 4\pi\Sigma$, where $\langle B^2 \rangle = \int B^2 dz$ is the vertically-integrated square of the magnetic field. The sound speed $c_s^2 = d\langle P \rangle / d\Sigma$, where $\langle P \rangle = \int P dz$. Terquem (2003) determines the strength of the magnetic field via $\beta_{v_A} = c_s^2 / v_A^2$, which is evaluated at the location of the planet.²

The locations of the resonances when the disc is Keplerian ($\Omega \approx \Omega_K$) and thin ($H/r \ll 1$) are given by

$$|r_M - r_p| = \frac{2H}{3\sqrt{1 + \beta_{v_A}}}, \quad (3)$$

where the thickness of the disc H and the plasma parameter $\beta_{v_A} = c_s^2 / v_A^2$ are evaluated at $r = r_p$. As the field becomes weaker (i.e., $\beta_{v_A} \rightarrow \infty$), the magnetic resonances converge toward the corotation radius. We suggest that $c_s / (r\Omega) \approx H/r$ and find the position of the inner and outer magnetic resonances to be

$$r_{\text{IMR}} = r_p - \frac{2H}{3\sqrt{1 + \beta_{v_A}}}, \quad r_{\text{OMR}} = r_p + \frac{2H}{3\sqrt{1 + \beta_{v_A}}}. \quad (4)$$

Terquem (2003) showed that the waves associated with the magnetic resonances can exert a positive torque on the planet that is larger in magnitude than the differential Lindblad torque if the magnetic field increases toward the star.

Fromang et al. (2005) performed simulations of a planet’s migration in a magnetized disc and found that the magnetic resonances can slow or stop the migration of a planet. In particular, they investigated the migration of a $5M_\oplus$ planet embedded in a disc that is threaded with an azimuthal

² In our simulations, we use the standard definition of the plasma parameter, $\beta = 2\beta_{v_A}$.

magnetic field with $B_\varphi \propto r^{-k}$ with $\Sigma = \text{const}$ initially. They took an initial value of $\beta_{v_a} = 2$ at the planet's location and found that, depending on the steepness of the magnetic field distribution (defined by k), the planet's migration slowed or reversed in direction.

Guilet et al. (2013) studied the effects of an MHD corotation torque on a low-mass planet in a 2D laminar disc with a weak azimuthal field threading the disc. The field was not strong enough to generate an appreciable torque from magnetic resonances, and it was not strong enough to dominate the hydrodynamic corotation torques, but a "torque excess" attributed to the presence of the magnetic field was found.

2.2.2 Migration in a turbulent disc

The MRI arises under conditions in which a weak magnetic field threads the disc and the radial component of the field can be stretched and enhanced by the differential rotation in the disc. Such a seed field can either be an axial field, perpendicular to the disc (Balbus & Hawley 1991, 1998), or an azimuthal field (Terquem & Papaloizou 1996). Below, we briefly summarize the conditions for the onset of the MRI instability in these two cases.

Axial Seed Magnetic Field.

Balbus & Hawley (1991) considered the case in which an axial magnetic field, $B_0 \hat{z}$, threads a Keplerian disc that rotates with an angular speed Ω . For axisymmetric perturbations of the disc, for which $\delta \mathbf{v} = [\delta v_r(z, t), \delta v_\varphi(z, t), 0]$ and $\delta \mathbf{B} = [\delta B_r(z, t), \delta B_\varphi(z, t), 0]$, and for perturbations proportional to $\exp(ik_z z - i\omega t)$, one finds the dispersion relation

$$\omega_\pm^2 = (k_z v_A)^2 + \frac{1}{2} \kappa_r^2 \pm \left[\frac{1}{4} \kappa_r^4 + 4(k_z v_A \Omega)^2 \right]^{1/2}, \quad (5)$$

where $v_A \equiv B_0 / \sqrt{4\pi\rho}$ is the Alfvén velocity, and

$$\kappa_r \equiv [4\Omega^2 + 2r\Omega d\Omega/dr]^{1/2} \quad (6)$$

is the radial epicyclic frequency of the disc. In order for the perturbation to fit within the vertical extent of the disc, one needs $k_z h \gtrsim 1$, where $h = c_s/\Omega$ is the half-thickness of the disc and c_s is the isothermal sound speed in the disc. For most conditions, the disc is thin, with $h \ll r$ or $c_s \ll r\Omega$.

Evidently, instability can occur if $\omega^2 < 0$, which happens if $(k_z v_A)^2 < -r\Omega d\Omega^2/dr$. For a Keplerian disc, this corresponds to $(k_z v_A)^2 < 3\Omega^2$. Therefore, the above-mentioned condition that $k_z h \gtrsim 1$ implies that instability occurs only for $v_A < c_s$.

Toroidal seed magnetic field.

Terquem & Papaloizou (1996) studied the linear MHD stability/instability of a thin Keplerian disc with a toroidal magnetic field $B_\varphi(r, z)$. This case is more complicated than the case of a vertical field (Balbus & Hawley 1998).

The complication in the toroidal field case results from the presence of both the MRI instability and the buoyancy instability of the toroidal field (Hoyle & Ireland 1960; Parker 1966). The buoyancy instability is triggered by an azimuthally-dependent, radially-localized vertical displacement in the plasma and the toroidal field (Terquem & Papaloizou 1996). These authors find that the MRI instability in a thin disc with an embedded toroidal magnetic field shows up in localized perturbations (i.e., whose wavelengths are

small compared with r), $\propto \exp(ik_r r + im\varphi + ik_z z - i\omega t)$, under the conditions $k_z^2 \gg k_r^2$ and $(k_\varphi v_A)^2 < -rd\Omega^2/dr$, where $k_\varphi = m/r$. This is the same as the condition for the MRI instability in a disc threaded by a vertical field with $B_z \rightarrow B_\varphi$ and $k_z \rightarrow k_\varphi$. Therefore, perturbations of the azimuthal field may also lead to MRI turbulence.

Work done by Baruteau et al. (2011) and Uribe et al. (2011) showed the existence of additional MHD corotation torques in MRI-turbulent discs using 3D MHD simulations. Furthermore, Nelson & Papaloizou (2004) investigated planet migration in an MRI-turbulent disc and observed stochastic migration. However, the origin of the torque on the planet in a turbulent disc is not well studied.

3 MODEL

3.1 MHD Equations

We utilize the MHD equations to numerically evaluate the perturbative effect of the planet on the disc:

(i) Continuity equation (conservation of mass)

$$\frac{\partial \Sigma}{\partial t} + \frac{1}{r} \frac{\partial}{\partial r} (r \Sigma v_r) + \frac{1}{r} \frac{\partial}{\partial \varphi} (\Sigma v_\varphi) = 0, \quad (7)$$

where $\Sigma = \int \rho dz$ is the surface density (with ρ the volume density), and v_r and v_φ are the radial and azimuthal velocities, respectively.

(ii) Radial equation of motion (conservation of momentum)

$$\begin{aligned} \frac{\partial}{\partial t} (\Sigma v_r) + \frac{1}{r} \frac{\partial}{\partial r} \left[r \left(\Sigma v_r^2 + \Pi + \frac{\Psi_{rr} + \Psi_{\varphi\varphi}}{8\pi} - \frac{\Psi_{r\varphi}}{4\pi} \right) \right] \\ + \frac{1}{r} \frac{\partial}{\partial \varphi} \left(\Sigma v_r v_\varphi - \frac{\Psi_{r\varphi}}{4\pi} \right) \\ = \frac{\Pi}{r} + \frac{\Psi_{rr} + \Psi_{\varphi\varphi}}{8\pi r} - \Sigma \frac{GM_\star}{r^2} + \Sigma w_r, \end{aligned} \quad (8)$$

where $\Pi = \int P dz$ is the surface pressure (with P the volume pressure), Σw_r is the radial force exerted on the disc by the planet (per unit area of the disc), and Ψ_{rr} , $\Psi_{r\varphi}$, and $\Psi_{\varphi\varphi}$ are magnetic surface variables that are discussed in more detail in §3.1.1.

(iii) Azimuthal equation of motion (conservation of angular momentum)

$$\begin{aligned} \frac{\partial}{\partial t} (\Sigma v_\varphi) + \frac{1}{r^2} \frac{\partial}{\partial r} \left[r^2 \left(\Sigma v_r v_\varphi - \frac{\Psi_{r\varphi}}{4\pi} \right) \right] \\ + \frac{1}{r} \frac{\partial}{\partial \varphi} \left(\Sigma v_\varphi^2 + \Pi + \frac{\Psi_{rr} + \Psi_{\varphi\varphi}}{8\pi} - \frac{\Psi_{r\varphi}}{4\pi} \right) \\ = \Sigma w_\varphi, \end{aligned} \quad (9)$$

where Σw_φ is the azimuthal force exerted on the disc by the planet (per unit area of the disc).

(iv) Radial induction equation

$$\frac{\partial \Phi_r}{\partial t} + \frac{1}{r} \frac{\partial}{\partial \varphi} (v_\varphi \Phi_r - v_r \Phi_\varphi) = 0, \quad (10)$$

where Φ_r and Φ_φ are magnetic surface variables, also discussed in §3.1.1.

(v) Azimuthal induction equation

$$\frac{\partial \Phi_\varphi}{\partial t} + \frac{\partial}{\partial r} (v_r \Phi_\varphi - v_\varphi \Phi_r) = 0. \quad (11)$$

(vi) Entropy balance equation

$$\frac{\partial}{\partial t}(\Sigma S) + \frac{1}{r} \frac{\partial}{\partial r}(r \Sigma S v_r) + \frac{1}{r} \frac{\partial}{\partial \varphi}(\Sigma S v_\varphi) = 0, \quad (12)$$

where $S = \Pi/\Sigma^\gamma$ is a function analogous to entropy, and we use $\gamma = 1.01$ so that our disc is isothermal. We chose an isothermal disc to ease comparisons of our results with the results of other authors (e.g., by Fromang et al. 2005).

Moreover, viscosity terms were added to the equations of motion following the α prescription of Shakura & Sunyaev (1973) (see details in Koldoba et al. 2015). We use a very small viscosity ($\alpha = 0.001$), analogous to Fromang et al. (2005), to isolate the effects of slow magnetosonic waves in the disc by smoothing out the effects of fast magnetosonic waves.

3.1.1 Magnetic surface variables

The “volume” values for the radial and azimuthal magnetic fields are given by B_r and B_φ . Their vertically-integrated counterparts may be defined similarly to Σ and Π as

$$\Phi_r = \int B_r dz \quad \text{and} \quad \Phi_\varphi = \int B_\varphi dz, \quad (13)$$

respectively. There are also terms in the MHD equations involving magnetic flux or energy that involve products of these variables: B_r^2 , B_φ^2 , and $B_r B_\varphi$. We define the following vertically-integrated quantities for these products,

$$\Psi_{rr} = \int B_r^2 dz, \quad \Psi_{\varphi\varphi} = \int B_\varphi^2 dz, \quad \text{and} \quad \Psi_{r\varphi} = \int B_r B_\varphi dz, \quad (14)$$

respectively.

As shown in Eqns. (8) - (11), the induction equations use Φ_r and Φ_φ , while the equations of motion use Ψ_{rr} , $\Psi_{r\varphi}$, and $\Psi_{\varphi\varphi}$. As such, we need a way to relate Φ and Ψ . We can do this by introducing a “magnetic” thickness of the disc, h_m . Using the definitions of Φ and Ψ , with h_m , we find that

$$\Psi_{rr} = \frac{\Phi_r \Phi_r}{h_m}; \quad \Psi_{r\varphi} = \frac{\Phi_r \Phi_\varphi}{h_m}; \quad \Psi_{\varphi\varphi} = \frac{\Phi_\varphi \Phi_\varphi}{h_m}. \quad (15)$$

We suggest that the value of $h_m = \text{const}$ is the same in all three relations. By relating Φ and Ψ in this way, we can define a “surface magnetic field”, \mathfrak{B} , such that the MHD equations are parameterized with respect to a single magnetic field variable,

$$\mathfrak{B}_r = \frac{\Phi_r}{\sqrt{h_m}} \quad \text{and} \quad \mathfrak{B}_\varphi = \frac{\Phi_\varphi}{\sqrt{h_m}}. \quad (16)$$

Then, the magnetic terms in Equations (8) - (11) take their usual form.

The radial equation of motion becomes

$$\begin{aligned} \frac{\partial}{\partial t}(\Sigma v_r) &+ \frac{1}{r} \frac{\partial}{\partial r} \left[r \left(\Sigma v_r^2 + \Pi + \frac{\mathfrak{B}_r^2 + \mathfrak{B}_\varphi^2}{8\pi} - \frac{\mathfrak{B}_r^2}{4\pi} \right) \right] \\ &+ \frac{1}{r} \frac{\partial}{\partial \varphi} \left(\Sigma v_r v_\varphi - \frac{\mathfrak{B}_r \mathfrak{B}_\varphi}{4\pi} \right) \\ &= \frac{\Sigma v_\varphi^2}{r} + \frac{\Pi}{r} + \frac{\mathfrak{B}_r^2 + \mathfrak{B}_\varphi^2}{8\pi r} \\ &- \Sigma \frac{GM_\star}{r^2} + \Sigma w_r, \end{aligned} \quad (17)$$

and the azimuthal equation of motion becomes

$$\begin{aligned} \frac{\partial}{\partial t}(\Sigma v_\varphi) &+ \frac{1}{r^2} \frac{\partial}{\partial r} \left[r^2 \left(\Sigma v_r v_\varphi - \frac{\mathfrak{B}_r \mathfrak{B}_\varphi}{4\pi} \right) \right] \\ &+ \frac{1}{r} \frac{\partial}{\partial \varphi} \left(\Sigma v_\varphi^2 + \Pi + \frac{\mathfrak{B}_r^2 + \mathfrak{B}_\varphi^2}{8\pi} - \frac{\mathfrak{B}_\varphi^2}{4\pi} \right) \\ &= \Sigma w_\varphi. \end{aligned} \quad (18)$$

The radial and azimuthal induction equations become, respectively,

$$\frac{\partial \mathfrak{B}_r}{\partial t} + \frac{1}{r} \frac{\partial}{\partial \varphi} (v_\varphi \mathfrak{B}_r - v_r \mathfrak{B}_\varphi) = 0 \quad (19)$$

and

$$\frac{\partial \mathfrak{B}_\varphi}{\partial t} + \frac{\partial}{\partial r} (v_r \mathfrak{B}_\varphi - v_\varphi \mathfrak{B}_r) = 0. \quad (20)$$

3.2 Planetary equation of motion

We calculate the equations of motion in the stellar reference frame, which is not inertial because the star also revolves about the center of mass of the system. So, an inertial force term is added to the equation of motion for both the disc and the planet. Assuming that the inertial acceleration is only due to the gravitational attraction between the star and the planet (but not the disc), the inertial force per unit mass (i.e., acceleration) is

$$\mathbf{w}_i = -\frac{GM_p}{r_p^3} \mathbf{r}_p. \quad (21)$$

To describe the gravitational influence of the planet on the disc, we use a gravitational potential similar to that used by Fromang et al. (2005),

$$\Phi_p = -\frac{GM_p}{\sqrt{r^2 + r_p^2 - 2rr_p \cos(\varphi - \varphi_p) + \epsilon^2}}, \quad (22)$$

where $\epsilon = 0.1H$ is the gravitational smoothing length, and H is the scale height of the disc. The total force per unit mass is

$$\mathbf{w} = \mathbf{w}_p + \mathbf{w}_i, \quad \mathbf{w}_p = -\nabla \Phi_p. \quad (23)$$

The components of this force in polar coordinates, w_r and w_φ , are used in Eqs. (17) and (18).

The force exerted on the planet by a particular fluid element with mass $dM = \Sigma r dr d\varphi$, is the acceleration given in Eqn. (23), with opposite sign, multiplied by the mass of the fluid element,

$$d\mathbf{f}_{\text{disc} \rightarrow \text{p}} = -dM \mathbf{w}_p = dM \nabla \Phi_p. \quad (24)$$

We then calculate the total force exerted on the planet by the disc by integrating over the disc within the computational domain,

$$\mathbf{F}_{\text{disc} \rightarrow \text{p}} = \int_{\text{disc}} d\mathbf{f}_{\text{disc} \rightarrow \text{p}} = \int_{\text{disc}} dM \nabla \Phi_p, \quad (25)$$

which we use to find the position (\mathbf{r}_p) and velocity (\mathbf{v}_p) of the planet at each time step via the planet’s equation of motion:

$$M_p \frac{d\mathbf{v}_p}{dt} = -\frac{GM_\star M_p}{r_p^3} \mathbf{r}_p - \frac{GM_p^2}{r_p^3} \mathbf{r}_p + \mathbf{F}_{\text{disc} \rightarrow \text{p}}. \quad (26)$$

The gravitational torque in the z direction on the planet is the sum over the torques from each fluid element:

$$T_z = \int_{\text{disc}} [\mathbf{r} \times d\mathbf{f}_{\text{disc} \rightarrow \text{p}}]_z. \quad (27)$$

We also calculate the planet's orbital energy and angular momentum per unit mass (e.g., Murray & Dermott 1999) via

$$E = \frac{1}{2}|\mathbf{v}_p|^2 - \frac{GM_\star}{r_p} \quad \text{and} \quad L = \mathbf{r}_p \times \mathbf{v}_p, \quad (28)$$

respectively. We use these relationships to calculate the semi-major axis and eccentricity of the planet's orbit at each time step,

$$a = -\frac{1}{2} \frac{GM_\star}{E} \quad \text{and} \quad e = \sqrt{1 - \frac{L^2}{GM_\star a}}, \quad (29)$$

respectively.

3.3 Initial conditions

The initial conditions for the surface density, surface pressure and surface “magnetic field” are defined to be power laws

$$\Sigma = \Sigma_i \left(\frac{r}{r_i} \right)^{-n}, \quad (30)$$

$$\Pi = \Pi_i \left(\frac{r}{r_i} \right)^{-l}, \quad \text{and} \quad (31)$$

$$\mathfrak{B}_\varphi = \mathfrak{B}_{\varphi,i} \left(\frac{r}{r_i} \right)^{-k}, \quad (32)$$

where r_i is a characteristic radius in the disc; in most of our simulations $r_i = r_{p,i}$ is the initial location of the planet. Additionally, n , l , and k are the power laws in the density, pressure, and magnetic field distributions, respectively. We suggest that the initial pressure distribution is similar to the initial density distribution (i.e., $n = l$). The initial sound speed in the disc at r_i , defined as a fraction of the Keplerian speed at this radius, k_s , is

$$c_i^2 = k_s \frac{GM_\star}{r_i}, \quad (33)$$

where $k_s = 0.01$. The initial surface pressure at r_i is $\Pi_i = \Sigma_i c_i^2$. The initial plasma parameter at r_i is then defined as

$$\beta_i = \frac{8\pi\Pi_i}{\mathfrak{B}_{\varphi,i}^2}. \quad (34)$$

Note again that this plasma parameter, β_i , is twice as large as the plasma parameter defined in Fromang et al. (2005). We determine the surface magnetic field distribution via

$$\mathfrak{B}_{\varphi,i} = \sqrt{\frac{8\pi\Pi_i}{\beta_i}}. \quad (35)$$

We determine the initial equilibrium in the disc from the force balance in the radial direction:

$$-\frac{v_\varphi^2}{r} + \frac{1}{\Sigma} \frac{d\Pi}{dr} + \frac{1}{8\pi r^2 \Sigma} \frac{d(r\mathfrak{B}_\varphi)^2}{dr} + \frac{GM_\star}{r^2} = 0. \quad (36)$$

It is satisfied if the initial distribution of the azimuthal velocity has the form

$$v_\varphi^2 = \frac{GM_\star}{r} + c_i^2 \left(\frac{r}{r_i} \right)^n \left[-n \left(\frac{r_i}{r} \right)^n + \frac{1-k}{\beta_i} \left(\frac{r_i}{r} \right)^{2k} \right]. \quad (37)$$

For all of the simulations presented here, we took $k_s = 0.01$. The thickness of the disc at r_i is $H_i = \sqrt{k_s r_i}$. The smoothing radius of the gravitational potential is $\epsilon = 0.1H$. An initial plasma parameter of $\beta_i = 1, 2$ is taken for analysis of migration in laminar MHD discs, while we increase β_i up to

Variable Definitions

r_0	Reference distance
v_0	Reference velocity
P_0	Reference orbital period
M_{d0}	Reference disc mass
Σ_0	Reference surface density
B_0	Reference magnetic field strength
T_0	Reference torque per unit mass

(a)

Standard reference values

	$r_0 = 0.1 \text{ AU}$	$r_0 = 1 \text{ AU}$
v_0	94.1 km s ⁻¹	29.8 km s ⁻¹
P_0	11.6 days	367 days
M_{d0}	1 M_\odot	1 M_\odot
Σ_0	$8.84 \times 10^8 \text{ g cm}^{-2}$	$8.84 \times 10^6 \text{ g cm}^{-2}$
B_0	228 kG	2.28 kG
T_0	$8.85 \times 10^{13} \text{ cm}^2 \text{ s}^{-2}$	$8.85 \times 10^{12} \text{ cm}^2 \text{ s}^{-2}$

(b)

Rescaled reference values

	$r_0 = 0.1 \text{ AU}$	$r_0 = 1 \text{ AU}$
v_0	94.1 km s ⁻¹	29.8 km s ⁻¹
P_0	11.6 days	367 days
M_{d0}	$10^{-3} M_\odot$	$10^{-3} M_\odot$
Σ_0	$8.84 \times 10^5 \text{ g cm}^{-2}$	$8.84 \times 10^3 \text{ g cm}^{-2}$
B_0	7.22 kG	72.2 G
T_0	$8.85 \times 10^{13} \text{ cm}^2 \text{ s}^{-2}$	$8.85 \times 10^{12} \text{ cm}^2 \text{ s}^{-2}$

(c)

Table 1. Example reference units calculation. The stellar mass is $M_\star = 1M_\odot$. (a) Definitions of the variables used. (b) Standard reference values, corresponding to $\tilde{\Sigma} = 1$. (c) Rescaled reference values, corresponding to $\tilde{\Sigma} = 0.001$, which is the value used in the code.

$\beta_i = 100$ to study migration in a turbulent disc. We consider the migration of a $5M_\oplus$ planet in most of the simulations, as well as a $20M_\oplus$ planet in a few simulations.

3.4 Reference Units

Our simulations are performed using dimensionless units $\tilde{A} = A/A_0$ where A_0 are the reference units. We first choose some reference distance, r_0 . The results of our simulations are applicable to multiple regions in a protoplanetary disc, because r_0 can be chosen to correspond to different regions of the disc. In Table 1, we show examples of reference values for scale distances of $r_0 = 0.1 \text{ AU}$ and $r_0 = 1 \text{ AU}$. The thickness of the disc is $H = 0.1r_0$. We take the mass of the star, $M_\star = 1M_\odot$, and determine the reference velocity, which is the Keplerian velocity at r_0 , $v_0 = \sqrt{GM_\star/r_0}$. The reference time is $t_0 = r_0/v_0$, and we use the reference orbital period $P_0 = 2\pi t_0$ as the unit of time in our plots.

We next define the reference mass of the disc M_{d0} : $M_{d0} = M_\star$. We then introduce the reference surface density, Σ_0 , such that $M_{d0} = \Sigma_0 r_0^2$. When the disc is homogeneous (i.e., $\Sigma = \text{const}$), M_{d0} is the mass of the disc inside $r = r_0$. The reference surface pressure is $\Pi_0 = \Sigma_0 v_0^2$.

The reference surface magnetic field is derived from the condition $\Sigma_0 v_0^2 = \mathfrak{B}_0^2$. Hence, $\mathfrak{B}_0 = \sqrt{\Sigma_0 v_0^2}$. Taking into account our definitions of the surface magnetic field (see Eqns. 13 and 14), we obtain the reference volume magnetic field: $B_0 = \mathfrak{B}_0 / \sqrt{r_0}$. The reference torque per unit mass is defined as $T_0 = r_0^2 / t_0^2$. These reference units are used to convert equations from dimensionless units. We show examples in Table 1b.

In our model, we use a small value of the dimensionless density $\tilde{\Sigma} = 0.001$; as a result, our dimensional characteristic disc mass is $M_{d0} = 10^{-3} M_\odot$. The other characteristic values are closer to realistic values and are much smaller than the reference values shown in Table 1b. We show in Table 1c the typical dimensional values corresponding to our simulations. One can see that, in the case of $r_0 = 1$ AU, the surface density and other parameters are close to those expected in real protoplanetary discs. The values shown for $r_0 = 0.1$ AU are too large, but we keep these model parameters for all distances in order to compare our results with those in Fromang et al. (2005) and others.³ From this point forward, we will use only dimensionless units and remove tildes from variables.

3.5 Grid and boundary conditions

We use a polar grid that is uniform in the φ direction. In the r direction, however, the grid is non-uniform; the size of the grid cells increases with radius such that the sides are approximately square-shaped throughout the disc. N_r is defined to be the number of radial grid cells, and N_φ is the number of azimuthal grid cells. Our grid consists of $N_r = 480$ and $N_\varphi = 1200$ cells. Our inner boundary is at $r_{\text{in}} = 0.4r_{p,i}$, and our outer boundary is at $r_{\text{out}} = 5r_{p,i}$.

We apply a wave damping procedure near both boundaries similar to that used in §3.1.3 of Fromang et al. (2005) to avoid high-amplitude wave reflections that can overwhelm the migration signal. We perform damping after every time step for $r < r_{\text{damp,in}}$, and $r > r_{\text{damp,out}}$, where $r_{\text{damp,in}} = 1.375r_{\text{in}}$ and $r_{\text{damp,out}} = 0.8r_{\text{out}}$. We calculate the velocities (v_r , v_φ), as well as Σ , Π , and S , using a method similar to Fromang et al. (2005),

$$\vec{\mathcal{J}} = \begin{cases} \mathcal{J}_{\text{in}} + (\mathcal{J} - \mathcal{J}_{\text{in}}) \exp \left[- \left(\frac{r - r_{\text{damp,in}}}{\delta_{\text{in}}} \right)^2 \right] & r < r_{\text{damp,in}} \\ \mathcal{J}_{\text{out}} + (\mathcal{J} - \mathcal{J}_{\text{out}}) \exp \left[- \left(\frac{r - r_{\text{damp,out}}}{\delta_{\text{out}}} \right)^2 \right] & r > r_{\text{damp,out}} \\ \mathcal{J} & \text{otherwise,} \end{cases} \quad (38)$$

where $\vec{\mathcal{J}} = (v_r, v_\varphi, \Sigma, \Pi, S)$, $\delta_{\text{in}} = 0.875r_{\text{in}}$, and $\delta_{\text{out}} = 0.8r_{\text{out}}$. Furthermore, \mathcal{J}_{in} and \mathcal{J}_{out} are the values of \mathcal{J} at the inner and outer disc boundaries, respectively.

³ It is often the case that the disc mass and the surface density are taken to be larger than in realistic discs. This leads to more rapid migration and thus shorter computational times (see, e.g., Armitage & Rice 2006).

Type	M_p (M_\oplus)	n	k	β_i	$r_{p,i}$	Name
Hydro	5	-1	—	—	1	H5n-1r1
Hydro	5	-0.5	—	—	1	H5n-0.5r1
Hydro	5	0	—	—	1	H5n0r1
Hydro	5	1	—	—	1	H5n1r1
Hydro	20	-1	—	—	1	H20n-1r1
Hydro	20	-0.5	—	—	1	H20n-0.5r1
Hydro	20	0	—	—	1	H20n0r1
<hr/>						
MHD	5	0	0	1	1	M5n0k0 β 1r1
MHD	5	0	0	2	1	M5n0k0 β 2r1
MHD	5	0	1	2	1	M5n0k1 β 2r1
MHD	5	0	2	2	1	M5n0k2 β 2r1
MHD	5	0	0	10	1	M5n0k0 β 10r1
MHD	5	0	0	100	1	M5n0k0 β 100r1
<hr/>						
MHD	5	1	0	2	1	M5n1k0 β 2r1
MHD	5	1	1	1	1	M5n1k1 β 1r1
MHD	5	1	1	2	1	M5n1k1 β 2r1
MHD	5	1	1	10	1	M5n1k1 β 10r1
MHD	5	1	2	2	1	M5n1k2 β 2r1
<hr/>						
MHD	20	0	0	2	1	M20n0k0 β 2r1
MHD	20	0	1	2	1	M20n0k1 β 2r1
MHD	20	0	2	2	1	M20n0k2 β 2r1
<hr/>						
Waves	5	0	—	—	2	W5n0k0r2
Waves	5	0	0	100	2	W5n0k0 β 100r2

Table 2. Simulation names and their respective distinguishing variables. See a more detailed description in §4.

4 PARAMETER SPACE

We calculated a number of models at different initial parameters, which are described below (see also Table 2):

Simulation type: The simulations are performed in a hydrodynamic disc or an MHD disc, or to study the interaction between the planet and waves in the disc.

Planet mass: We explored two different planet masses – $5M_\oplus$ and $20M_\oplus$.

Surface density exponent, n : This defines the initial surface density distribution in the disc, according to $\Sigma \propto r^{-n}$.

Surface magnetic field exponent, k : This defines the initial surface magnetic field distribution in the disc, according to $\mathfrak{B} \propto r^{-k}$.

Matter-to-magnetic pressure ratio, β_i : This defines the value of β_i at the initial location of the planet.

Initial planet location, $r_{p,i}$: This defines the initial orbital radius of the planet.

The last column of Table 2 shows the names of the simulations presented in subsequent sections. These names are referenced in the figure captions and related discussion.

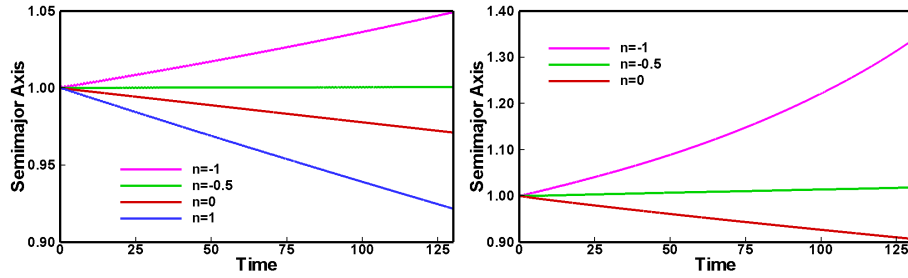


Figure 2. Left Panel: The variation in semimajor axis versus time for a $5M_{\oplus}$ planet embedded in a hydrodynamic disc for different values of n (where $\Sigma \propto r^{-n}$). The models shown include: H5n-1r1, H5n-0.5r1, H5n0r1, H5n1r1. Right Panel: A similar plot, but for a $20M_{\oplus}$ planet. The models shown include: H20n-1r1, H20n-0.5r1, H20n0r1.

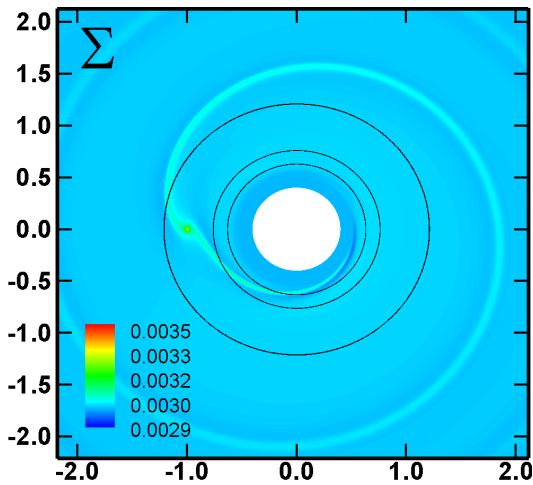


Figure 1. An example of a hydrodynamic simulation of migration corresponding to the model H5n0r1 after 10 orbits of the planet. The color background shows the surface density distribution. The $m = 1, 2$ Lindblad resonances are indicated by the solid black circles.

5 MIGRATION IN A HYDRODYNAMIC DISC

As a first step, we investigated the migration of a planet in a hydrodynamic disc with an initially homogeneous density distribution ($n = 0$); these simulations are used as a base for studying migration in magnetic discs. Fig. 1 shows the surface density distribution in the disc after 10 orbits of the planet. The planet excites two density waves at the inner and outer Lindblad resonances (which are shown as black circles in the figure).

As a next step, we considered different initial density distributions in the disc, $\Sigma \sim r^{-n}$ including those where the density is homogeneous, $n = 0$, increases towards the star, $n = 1$, or decreases toward the star, $n = -0.5, -1$. Fig. 2 (left panel) shows the variation of the planet's semimajor axis over time for these cases. We observed inward migration when $n = 0$ and more rapid inward migration when $n = 1$. When $n = -0.5$, the migration almost stalls (where only slow outward migration has been observed), and we observed more rapid outward migration when $n = -1$.

The migration rate and its direction are determined by the cumulative value of the Lindblad and corotation torques, as described in Sec. 2.1. When the density increases towards the star ($n = 1$) or the density is constant in the disc ($n = 0$), the Lindblad torque is larger than the corotation torque, and

the planet migrates towards the star. However, when the density decreases towards the star, $n = -1$, the corotation torque is larger than the Lindblad torque, and the planet migrates outwards. In the case of a more shallow positive density distribution, $n = -0.5$, the Lindblad and corotation torques are almost equal, and the cumulative torque is small.

The migration due to both the Lindblad and corotation torques has been studied in semi-analytical models by Tanaka et al. (2002). In two dimensions, they obtained the torque on the planet from the disc:

$$\Gamma_{\text{total},2D} = -(1.160 + 2.828\alpha) \left(\frac{M_p}{M_*} \frac{r_p \Omega_p}{c_s} \right)^2 \Sigma(r_p) r_p^4 \Omega_p^2, \quad (39)$$

where α defines the slope of the density distribution ($\Sigma \propto r^{-\alpha}$), and c_s is the isothermal sound speed in the disc at the orbital radius of the planet. This implies that the total torque on the planet in a two-dimensional disc is zero when $\alpha = -0.41$, suggesting that

- (i) the torque on the planet is positive, and the planet migrates outward, when $\alpha < -0.41$;
- (ii) the torque on the planet is zero, and the planet's migration halts, when $\alpha = -0.41$; and
- (iii) the torque on the planet is negative, and the planet migrates inward, when $\alpha > -0.41$.

The value of $n = -0.5$ obtained from our simulations is very close to the value $n = -0.41$ corresponding to zero torque derived by Tanaka et al. (2002) for two dimensions.

We also performed simulations of the migration of a $20M_{\oplus}$ planet. Fig. 2 (right panel) shows that the planet migrates inward when $n = 0$; almost no migration is observed when $n = -0.5$ (as with the $5M_{\oplus}$ planet); and the migration direction is outward when $n = -1$. These results are in accord with that of a $5M_{\oplus}$ planet, while the migration rate is faster in the $20M_{\oplus}$ case. This is expected according to Eqn. (39), which states that the total Lindblad torque increases with the mass of the planet.

Our simulations of hydrodynamic discs are in accord with theoretical studies (e.g., Tanaka et al. 2002) and simulations performed by others (see review by Kley & Nelson 2012).

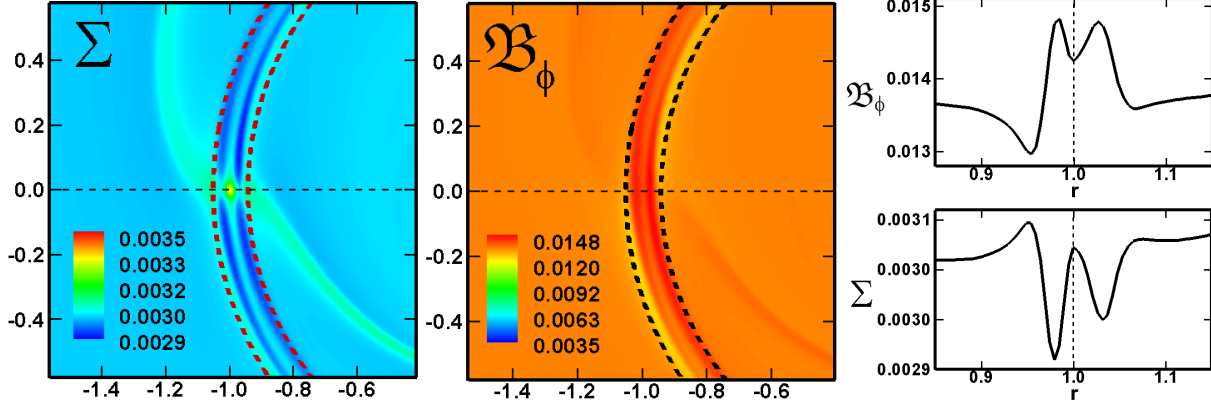


Figure 3. The surface density and surface azimuthal magnetic field distributions for the model M5n0k0β2r1 at $t = 10$. *Left Panel:* The two-dimensional surface density distribution. The dashed red lines show the positions of the magnetic resonances. *Middle Panel:* The two-dimensional surface azimuthal magnetic field distribution. The dashed black lines show the positions of the magnetic resonances. *Right Top Panel:* The one-dimensional surface azimuthal magnetic field distribution, taken along the horizontal dashed line in the left two panels.

Right Bottom Panel: The one-dimensional surface density distribution, taken along the horizontal dashed line in the left two panels. The vertical dashed line shows the location of the planet

6 MIGRATION IN LAMINAR DISC DUE TO MAGNETIC RESONANCES

6.1 Magnetic resonances in the case of a constant density distribution

We performed a series of simulations to investigate the influence of an ordered azimuthal magnetic field in the disc on a planet's migration. We started by investigating migration in discs with a homogeneous surface density distribution (i.e., $n = 0$), with initial and boundary conditions very similar to those used by Fromang et al. (2005). In particular, we considered an isothermal disc (i.e., $\gamma = 1.01$) and set the strength of the magnetic field near the planet such that $\beta_i = 2$. Our goal was to see whether our code can reproduce the results presented by Fromang et al. (2005).

First, we investigated a homogeneous magnetic field (i.e., $k = 0$). Fig. 3 shows an example simulation after 10 orbital periods of the planet. We observed that the planet excites ring-like waves at which the azimuthal magnetic field is stronger and the surface density is lower than in other nearby regions in the disc. These locations correspond to the magnetic resonances that are excited by slow magnetosonic waves propagating along the field lines. Fig. 3 shows two rings of lower density (left panel), corresponding to two rings of enhanced azimuthal field (middle panel). The position of the magnetic resonances is similar to that found in the simulations by Fromang et al. (2005), and they correspond to the theoretical resonance locations predicted by Terquem (2003) (see the dashed-line circles in Fig. 3). The right panel shows the linear distribution of B_ϕ and Σ in the radial direction.

According to the theory presented by Terquem (2003), these waves exert a torque on the planet that can reverse the planetary migration direction if the magnetic field distribution is steep enough. We varied the steepness of the magnetic field, k (see Eq. 32), taking $k = 0, 1$ and 2 , and we obtained different migration rates. Fig. 4 (left panel) shows that, for a constant magnetic field distribution ($k = 0$), the planet migrates inwards but more slowly than in the purely hydrodynamic case. When $k = 1$, the planet slowly migrates outward,

while the planet migrates outward more rapidly when $k = 2$. These simulations confirm the result presented by (Fromang et al. 2005): in discs with a relatively strong azimuthal magnetic field, the magnetic resonances can slow or reverse a planet's migration.

6.2 Migration due to magnetic resonances for different density distributions

Next, we investigated the action of the magnetic resonances at different surface density distributions. First, we took a density distribution such that the density in the disc increases towards the star, $n = 1$, and repeated the above simulations at $k = 0, 1, 2$. Fig. 4 (middle panel) shows that the planet migrates inward in all three cases and, therefore, that the torque from the magnetic resonances is small compared with the differential Lindblad torque. The migration rate in the case of $k = 1$ almost exactly coincides with the purely hydrodynamic case. For a very steep magnetic field distribution, $k = 2$, the accretion rate is only slightly slower than for $k = 1$. Overall, we conclude that, in the case of this density distribution ($n = 1$), the positive torque associated with the magnetic resonances is not strong enough to overcome the negative differential Lindblad torque.

In another example, we considered a disc whose density decreases towards the star, $n = -0.5$. This situation is possible, for example, at the inner edge of the disc where the expanding magnetosphere or erosion of the disc may push the inner disc away from the star (e.g., Lovelace et al. 2008). When $n = -0.5$, the migration rate in the hydrodynamic case is very low (see Fig. 2, top panel) because the negative differential Lindblad torque is approximately compensated by the positive corotation torque. For this surface density distribution ($n = -0.5$), the positive torque associated with the magnetic resonances leads to outward migration of the planet, even for a flat magnetic field distribution, $k = 0$ (see Fig. 4, right panel). For a steeper magnetic field distribution, $k = 1$, the planet migrates outward even more rapidly. It appears, then, that magnetic torques may play a significant role at the

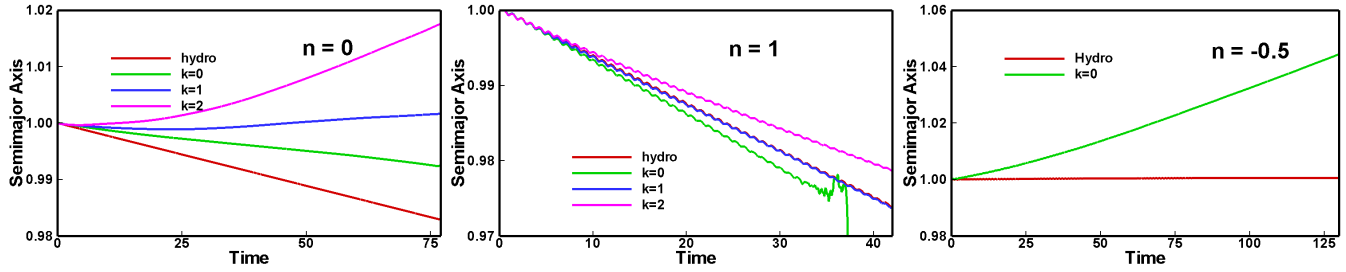


Figure 4. Change in semimajor axis versus time for a $5M_{\oplus}$ planet embedded in an MHD disc for different values of k (where $\mathcal{B} \propto r^{-k}$) and $\beta_i = 2$. The result for a hydrodynamic disc is shown for reference. *Left Panel:* Result shown for $n = 0$, corresponding to models H5n0r1, M5n0k0 β 2r1, M5n0k1 β 2r1, and M5n0k2 β 2r1. *Middle Panel:* Result shown for $n = 1$, corresponding to models H5n1r1, M5n1k0 β 2r1, M5n1k1 β 2r1, M5n1k2 β 2r1. *Right Panel:* Result shown for $n = -0.5$, corresponding to models H5n-0.5r1 and M5n-0.5k0 β 2r1.

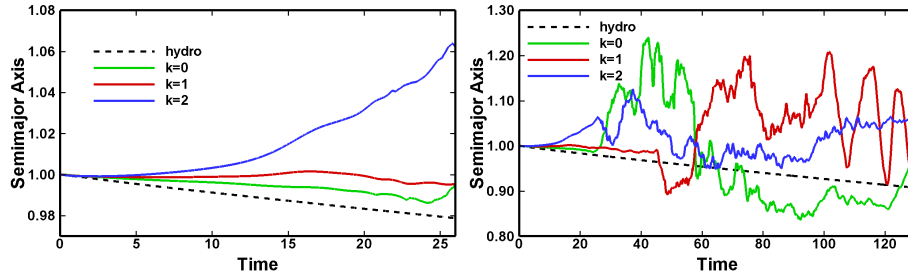


Figure 5. *Left Panel:* Variation of the semimajor axis of a $20M_{\oplus}$ planet under the influence of Lindblad and magnetic resonances for various values of initial surface magnetic field exponent, k , for the case $n = 0$ and $\beta_i = 2$, corresponding to models M20n0k0 β 2r1, M20n0k1 β 2r1, M20n0k2 β 2r1, and the hydrodynamic case H5n0r1. *Right Panel:* Same as in the left panel, but over a longer interval of time.

disc-cavity boundaries, as well as other regions where the surface density in the disc is flat or decreases towards the star.

We conclude that the rate and direction of migration are determined by the steepnesses of both the magnetic field distribution and the surface density distribution. If the surface density *increases* radially towards the star (e.g., $n = 1$), then the magnetic resonances do not exert enough torque to drive outward migration for any value of k . By contrast, when the surface density *decreases* toward the star (e.g., $n = -0.5$), the torque from the magnetic resonances is large enough to drive outward migration for different values of k . When the surface density is constant (i.e., $n = 0$), the magnetic resonances drive outward migration when $k = 1, 2$, and inward migration when $k = 0$.

6.3 Migration of a $20M_{\oplus}$ planet

The above analysis shows that the effect of an azimuthal magnetic field on a planet's migration strongly depends on both the surface density and magnetic field distributions in the disc. It is also interesting to investigate whether the magnetic resonances also depend on the mass of the planet. To investigate this issue, we simulated the migration of a $20M_{\oplus}$ planet in a magnetized disc with a flat surface density distribution ($n = 0$) and different steepnesses in the distribution of the magnetic field ($k = 0, 1, 2$). Fig. 5 (left panel) shows that, for a constant magnetic field in the disc, $k = 0$, the migration rate is slower than in the hydrodynamic case. For a steeper magnetic field distribution, $k = 1$, the inward migration is even slower, and the direction of the migration reverses at an even steeper field distribution, $k = 2$. These results are in general agreement with those obtained for a smaller-mass

planet: the magnetic resonances are strong enough to reverse the migration. Note that, at $k = 2$, the outward migration of the more massive planet is much faster than the migration of the lower-mass planet.

However, longer simulation runs have shown that, for a $20M_{\oplus}$ planet, the laminar stage of the disc does not last long, $\lesssim 10 - 40$ planetary orbits. At later times, the disc becomes turbulent. Fig. 5 (right panel) shows that, after a relatively brief stage of slow migration in the laminar disc, the migration becomes stochastic in the turbulent disc. We also see such a transition to stochastic migration for a $5M_{\oplus}$ planet, though at much later times ($t_{\text{turb}} \approx 80$ when $n = 0$, $k = 0$, and $\beta_i = 2$). In both cases, the disc becomes turbulent, and the semimajor axis varies in time stochastically due to the planet's interaction with turbulent cells in the disc.

We found that the observed turbulence is an interesting phenomenon and investigated the migration of planets in turbulent discs. Earlier, such migration was studied by Nelson & Papaloizou (2004) in 3D simulations; they observed that the migration becomes stochastic and the migration rate may be strongly modified or reversed due to interaction with turbulent cells in the disc. In this paper, we performed 2D simulations in polar coordinates, and we see similar stochastic migration of the planet due to interaction with turbulent cells in the disc. While 2D simulations of the MRI are somewhat restricted, they allow us an opportunity to investigate the details of the interaction between the planet and inhomogeneities in the disc. Below, we investigate migration in turbulent discs.

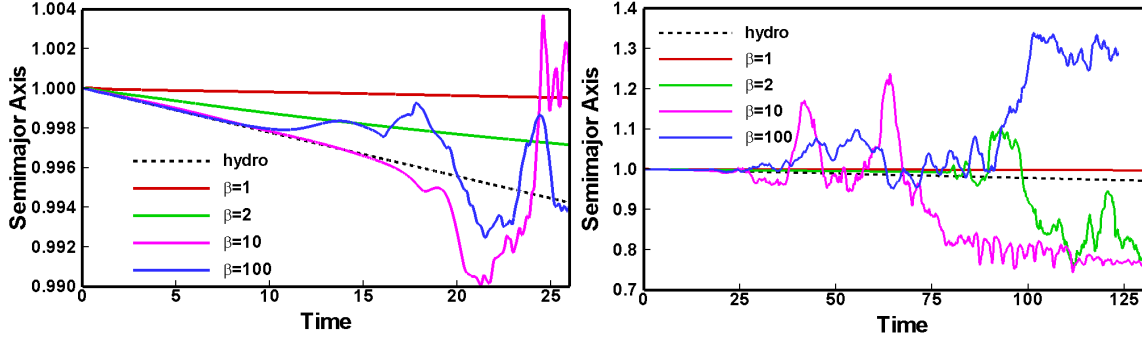


Figure 6. Left Panel: Variation of the semimajor axis of a $5M_{\oplus}$ planet for in models with different values of β_i when $n = 0$ and $k = 0$, corresponding to models H5n0r1, M5n0k0 β 1r1, M5n0k0 β 2r1, M5n0k0 β 10r1, and M5n0k0 β 100r1. Right Panel: Same as in the left panel, but over a longer interval of time.

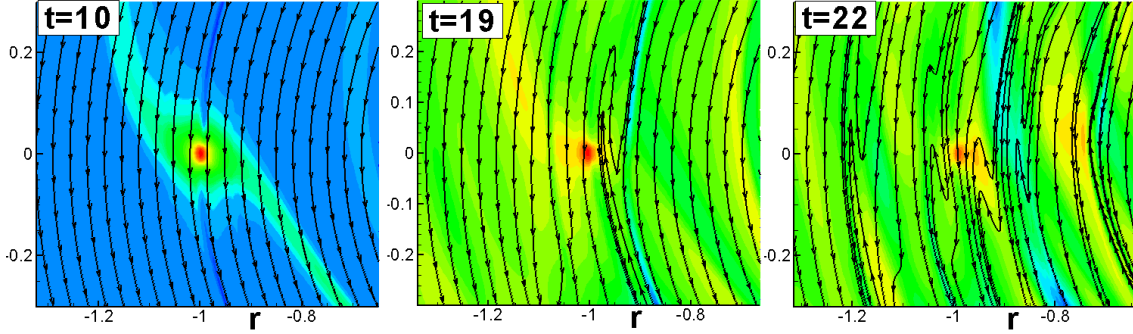


Figure 7. Surface density distribution and magnetic field lines corresponding to model M5n0k0 β 100r1 at $t = 10, 19, 22$. This figure demonstrates how initially-azimuthal field lines (left panel) acquire a radial component from non-axisymmetric matter flow near the planet (density waves) and start forming loops (middle panel). Later on, the process spreads to larger distances from the planet, forming an inhomogeneous distribution of matter and magnetic field in the disc (right panel).

7 MIGRATION IN A TURBULENT DISC

In this section, we investigate the transition from the laminar to the turbulent disc, the formation of turbulent discs, and the migration of a low-mass $5M_{\oplus}$ planet in discs with different strengths of the magnetic field. According to the theory of the MRI (see Sec. 2.2.2), instability is expected in magnetized discs with $\beta_i > 1$; that is, in discs in which the Alfvén velocity $v_A = B/\sqrt{4\pi\rho}$ is smaller than the sound speed c_s (e.g., Balbus & Hawley 1991, 1998; Terquem & Papaloizou 1996). Below, we show the results of simulations at different initial values of β_i (see Sec. 7.1) and the details of migration in the turbulent disc (see Sec. 7.2).

7.1 Migration in a turbulent disc with different β_i

We studied the migration of the planet in discs with different initial plasma parameters, $\beta_i = 1, 2, 10, 100$. Fig. 6 (left panel) shows that the disc is initially laminar, and the planet migrates smoothly. This period of smooth migration is longest when $\beta_i = 1$ and 2, but it is shorter for $\beta_i = 10$ and even shorter at $\beta_i = 100$. This is understandable, because the magnetic field is more easily tangled by the disc matter when the matter strongly dominates, such as when $\beta_i = 10$ and 100. The right panel of the same figure shows the semimajor axis of the planet at later times. One can see that the disc is still laminar when $\beta_i = 1$. In all other cases, the disc becomes turbulent. Note that the migration often changes direction from

inward to outward and vice versa; this reflects the stochastic nature of the migration process in a turbulent disc, as discussed below in Sec. 7.2.

7.2 Migration in a turbulent disc with $\beta_i = 100$

In this section, we consider the development of the MRI, as well as the migration of a planet in a turbulent disc, in greater detail. As a base, we consider a model where the initial value of plasma parameter is large, $\beta_i = 100$ (model M5n0k0 β 100), so that the MRI instability starts easily.

We observed that the origin of the radial component of the field, which is required for the instability, is in the fact that the planet excites non-axisymmetric waves in the disc. These waves lead to non-axisymmetric motion of the gas in the disc and, subsequently, to the formation of a radial component of the magnetic field, which is further stretched by the differential rotation in the disc. Fig. 7 shows how parts of the initially azimuthal magnetic field near the planet (left panel) acquire a radial component and are subsequently stretched by the differential rotation in the disc, eventually forming a loop (middle panel). Later, this process occurs at larger distances from the planet, many more field lines are stretched in the radial direction (such that different inhomogeneities and loops form), and the disc becomes globally inhomogeneous and turbulent.

Fig. 8 (left panel) shows that the disc consists of

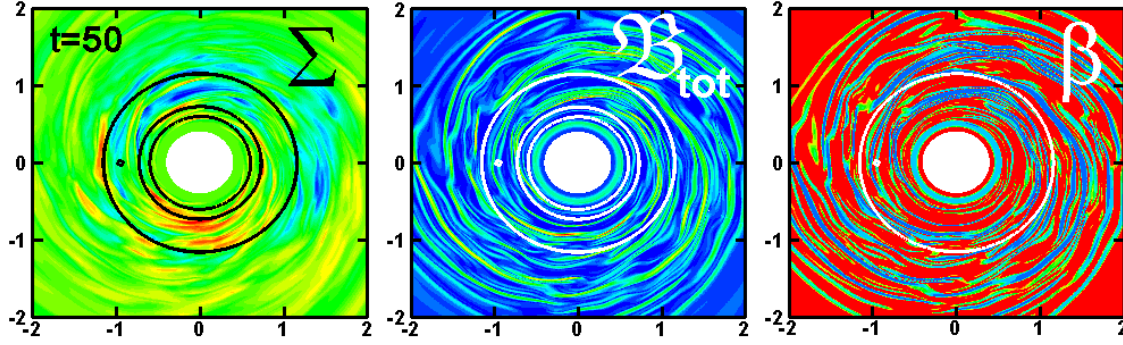


Figure 8. Planet migration in an MRI-turbulent disc in the model M5n0k0 β 100r1 at $t = 50$. *Left Panel:* The surface density variation in the inner part of the disc. The planet's location and the $m = 1$ and $m = 2$ Lindblad resonances are shown via the black circles. *Middle Panel:* The variation of the magnetic field magnitude (B_{tot}) in the inner part of the disc. The planet's location and the $m = 1$ and $m = 2$ Lindblad resonances are shown via the white circles. *Right Panel:* The variation of the plasma parameter (β_i) in the inner part of the disc. The planet's location and the $m = 1$ and $m = 2$ Lindblad resonances are shown via the white circles.

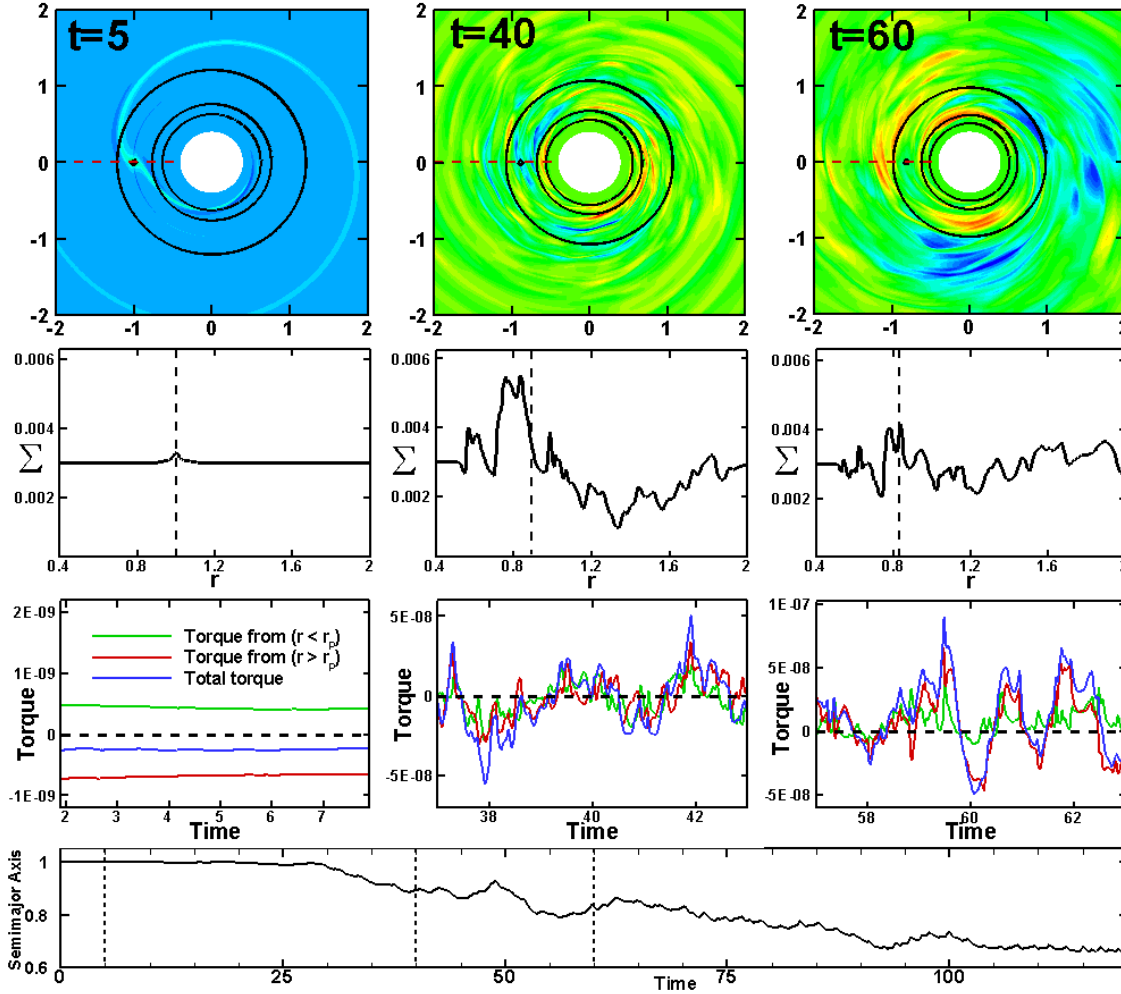


Figure 9. Planet migration in the model M5n0k0 β 100r1 shown for $t = 5, 40, 60$. *Top Panels:* The variation of the surface density (Σ) in the inner part of the simulation region. The location of the planet, and the $m = 1$ and $m = 2$ Lindblad resonances, are shown via the black circles. *Second Row of Panels from the Top:* The one-dimensional variation of the surface density along the red line in the panel above each respective plot. The vertical dashed black line shows the location of the planet. *Third Row of Panels from the Top:* The torques acting on the planet from the disc. The green line shows the torque on the planet from the disc where $r < r_p$, the red line shows the torque on the planet from the disc where $r > r_p$, and the blue line shows the total torque on the planet. The dashed black line marks zero torque. *Bottom Panel:* The change in the semimajor axis of the planet over time.

azimuthally-stretched turbulent cells. The middle panel of the same figure shows that the total magnetic field, B_{tot} , becomes strongly inhomogeneous, with some regions having the original polarity and others reversing polarity. The distribution of the plasma parameter, β_i , shows that the simulation region splits into regions that are either magnetically- or matter-dominated (right panel). Therefore, in the MRI regime, the disc becomes strongly inhomogeneous both in the density and in the magnetic field.

We investigated the density distribution, torque, and semimajor axis evolution of the planet in this case in greater detail. Fig. 9 (top panels) shows the surface density distribution in the disc at $t = 5, 40$ and 60 . At $t = 5$, the disc is still laminar and two Lindblad density waves are clearly seen. However, after $t \approx 10$, non-axisymmetric motions start to “tangle” the field lines of the weak magnetic field, and an MRI-type turbulence gradually develops. MRI-type turbulence is observed during the time interval $10 \lesssim t \lesssim 60$.

The middle column ($t = 40$) shows small-scale turbulent cells that persist for many orbits. However, later (at $t = 60$), the turbulent cells become larger in size because “islands” of stronger magnetic field also become larger in size, and often one or two main density waves form in the inner parts of the disc. The beginning of this process is seen in the right column of Fig. 9. We suggest that the finite life of the MRI turbulence and formation of these larger-scale waves may be connected with the 2D nature of our MRI turbulence. However, the low-amplitude MRI turbulence proceeds over long periods of time, which is sufficient to study the migration of a planet in the turbulent disc. Formation of large-scale waves is possible in realistic discs; we use these waves to study the interaction of a planet with waves in the disc in Sec. 8.

The second row in Fig. 9 shows the 1D density distribution along the line connecting the planet and the center of the star at the same times as the top row. When the disc is laminar, we see only a small bump in density associated with matter accumulation near the planet. However, as the disc becomes more and more turbulent, larger and larger variations in the surface density of the disc are observed.

The 3rd row in Fig. 9 shows the torques acting on the planet at the same times as the top two rows. When the disc is laminar (left column), the planet migrates due to the excitation of density waves at the Lindblad resonances: the inner torque is positive and smaller than the negative outer torque, so that the total torque is negative (the blue line in Fig. 9). In this case, the planet slowly migrates inward (see the slow variation of the semimajor axis up to time $t \approx 30$ in the bottom row). However, when the disc is turbulent ($t = 40, 60$), we observe that both the inner and outer torques can be either positive or negative; they both vary rapidly and the resulting torque also changes sign.

The *magnitudes* of these turbulent torques are much larger than those seen in the laminar case (note the torque magnitudes shown on the y -axes in the third row of Fig. 9). The torques become stochastic and correspond to the interaction of the planet with individual turbulent cells. The variation of the sign of the net torque shows also that the total averaged torque may be either negative or positive (i.e., that the direction of migration may change). In the shown example, the average total torque is negative and the planet migrates inward overall. Note that, in other cases, the direction

of the migration may be either inward or outward (see, e.g., Figs. 5 and 6).

8 INTERACTION BETWEEN A PLANET AND WAVES IN THE DISC

The interaction between a planet and turbulent cells in a disc is a complex process. The planet interacts with a set of turbulent cells gravitationally, but the Lindblad density waves are not homogeneous. The closest cell may contribute to the torque more strongly than more remote cells, and the torque becomes more stochastic. Additionally, the planet passes through individual cells, and each cell may exert a corotation torque on the planet. It is difficult to track the interaction of a planet with individual turbulent cells. That is why we developed conditions in which a planet interacts with ordered inhomogeneities (in the form of waves in the disc). We consider two types of waves: (1) low-amplitude ordered waves generated in a hydrodynamic disc by a force at the inner boundary (Sec. 8.1), and (2) high-amplitude waves that form at later times in simulations using an MHD disc (Sec. 8.2.)

8.1 Interaction between a planet and low-amplitude waves in a hydrodynamic disc

To better understand the interaction between a planet and individual turbulent cells, we created a model in which an ordered density wave is generated at the inner disc boundary by a periodic force that decreases with the radius as r^{-3} . This force generates density waves with a small amplitude, for which the density contrast between the wave and the disc is small, about 5 – 7%. The density wave then propagates through the simulation region. We placed a planet at an initial radius of $r_{p,i} = 2$, away from the action of this force at the boundary.

We observed that the planet moves faster than the wave and it interacts differently with different parts of the wave. Fig. 10 (top panels) shows slices of the surface density at $t = 12, 13, 14, 15, 16$. We show the moments when the planet is located at the inner or outer edge of a wave (i.e., where the surface density either decreases or increases toward the star, respectively). The corotation torque is larger than the differential Lindblad torque when the density slope in the disc corresponds to that in Equation (39); that is, the slope of the density distribution is either positive or only slightly negative toward the star (see Sec. 5). This is expected when the planet is at the inner edge of a wave.

The middle row of Fig. 10 shows the torques acting on the planet; the times from the top panels marked with vertical dashed lines. The total torque has maxima at $t = 12$ and $t = 15$. The top panels show that, at these moments of time, the planet is located at the inner edge of the wave and, therefore, that the positive torque acting on the planet is the corotation torque (which appears due to the positive density gradient at the inner edge of the wave). The bottom panel of Fig. 10 shows that the planet migrates inward overall, because the differential Lindblad torque dominates overall. However, at $t = 12$ and $t = 15$, the planet migrates outward due to the temporarily dominant corotation torque.

At $t = 13$ and $t = 16$, the planet is located at the outer

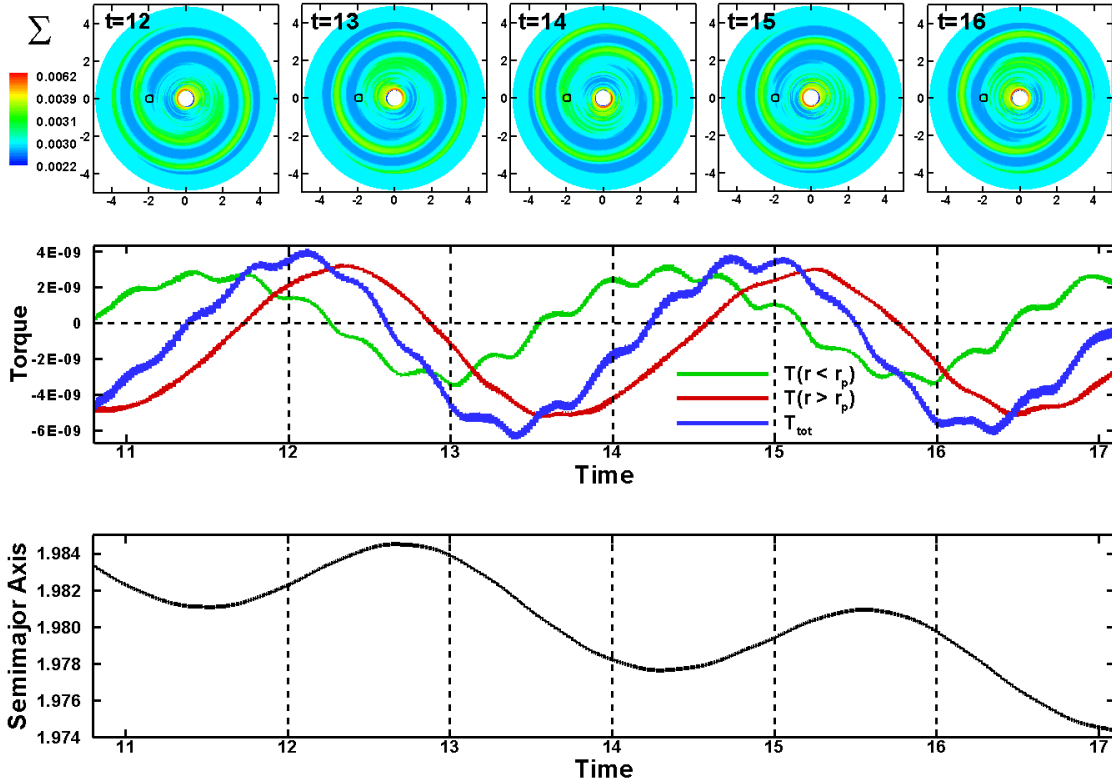


Figure 10. Migration of a $5M_{\oplus}$ planet in a hydrodynamic disc in the model W5n0r2, for which low-amplitude ordered density waves are propagated through the disc, at $t = 12, 13, 14, 15, 16$. The bottom two panels mark these times with vertical black dashed lines. *Top Panels:* The surface density (Σ) variation in the disc; the small black circle shows the location of the planet. *Middle Panel:* The torque on the planet from the disc. The green line shows the torque on the planet from the disc where $r < r_p$; the red line shows the torque on the planet from the regions of the disc where $r > r_p$, and the blue line shows the total torque on the planet. The horizontal dashed black line shows zero torque. *Bottom Panel:* The change in the semimajor axis of the planet over time.

edge of the density wave, where the density increases towards the star. At these moments of time, the total torque is negative and the planet migrates inward. We suggest that, at the outer edge of a wave, a planet excites density waves at the Lindblad resonances, and the differential Lindblad torque drives overall inward migration. However, when the planet is at the inner edge of the wave, the positive corotation torque is large, and the planet migrates outward.

8.2 Interaction between a planet and high-amplitude waves in an MHD disc

In this subsection, we analyze the passage of a planet through waves with much higher amplitudes. These high-amplitude waves often form at later times in simulations of MRI-turbulent discs, where the non-axisymmetry of the gravitational potential leads to the formation of the inner density waves. We chose the model where the initial plasma parameter $\beta_i = 100$ and a planet is placed at $r_{p,i} = 2$. At later moments in time, after the wave forms, the planet migrates to a radius of $r_p \approx 0.9 - 1$. Fig. 11 (top panels) shows the density distribution in the wave and the position of the planet for several representative moments in time, where the planet is located at the inner edge of a wave (left and right panels, $t = 180.25, 184.75$), the planet is in the middle of a wave ($t = 181.5$), and the planet is in the low-density region ($t = 183$). The density contrast between the wave and the rest

of the disc is $\sim 70\%$, which is about 10 times higher than the low-amplitude waves discussed in the previous subsection.

The middle and bottom rows of Fig. 11 show the torques acting on the planet and the variation of the planet's semimajor axis in time. The dashed vertical lines show the four moments in time corresponding to the top four panels. One can see that, at $t = 180.25$, the planet is located at the inner edge of the wave, where the density decreases towards the star, and the positive corotation torque is expected to be larger than the differential Lindblad torque. Indeed, the middle row shows that the total torque is positive at this moment of time, and the planet migrates outward.

At the second moment in time, $t = 181.5$, the planet is located in the middle of the density wave. The middle row shows that, at this moment, a strongly negative torque dominates, and the planet migrates inward. This large negative torque is primarily comprised of the differential Lindblad torque. This torque is proportional to the surface density in the disc, and therefore it is large when the planet is located inside the high-density wave. The positive corotation torque is relatively small. At $t = 183$, the planet is located away from the wave in the low-density part of the disc, and both torques are small. At the last considered moment ($t = 184.75$), the planet is again at the inner edge of the wave, where the corotation torque is positive and larger than the differential Lindblad torque, and the planet migrates outward.

In this example, the density wave is an analog of a large

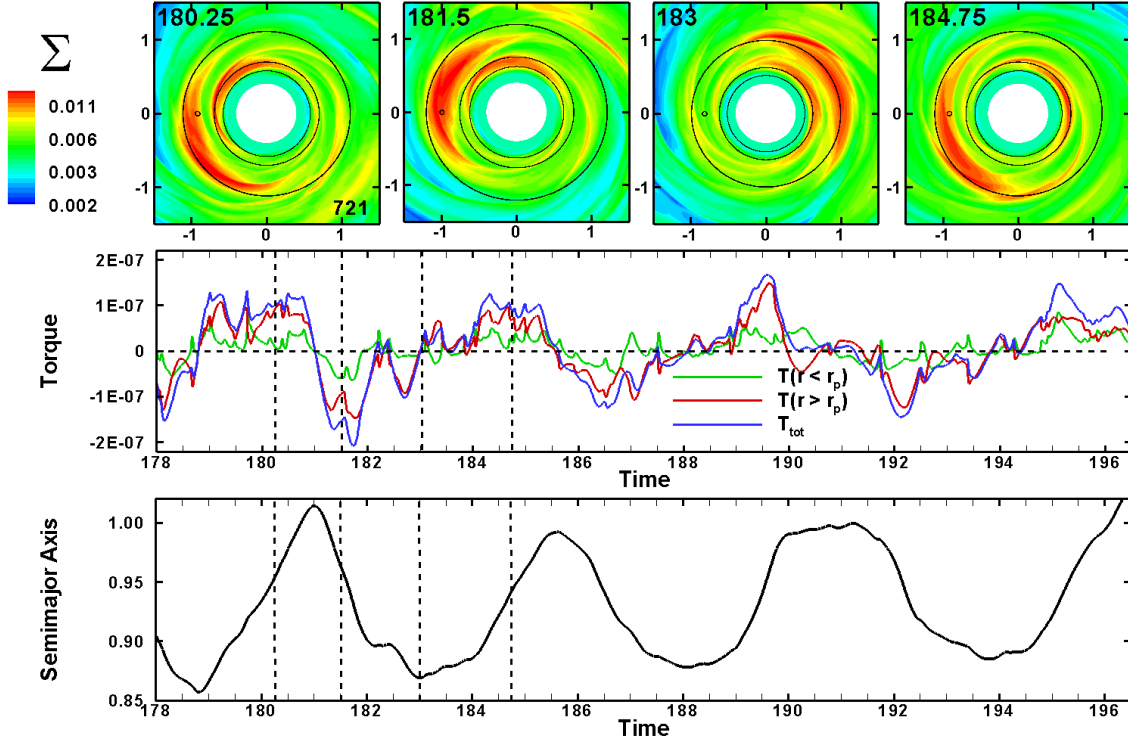


Figure 11. Planet migration in high-amplitude waves in the model W5n0k0 β 100r2 for $t = 180.25, 181.5, 183, 184.75$. In the two bottom panels, these times are shown by vertical black dashed lines. *Top Panels:* Surface density variation in the inner part of the simulation region. The large black circles show position of the Lindblad resonances, while the small black circle shows the position of the planet. *Middle Panel:* The torque on the planet from the disc. The green line shows the torque on the planet from the part of the disc where $r < r_p$; the red line shows the torque on the planet from the disc where $r > r_p$. The blue line shows the total torque on the planet. The horizontal dashed black line shows zero torque. *Bottom Panel:* The variation of the semimajor axis of the planet over time.

turbulent cell, where the total torque is either positive or negative and acts onto the planet depending on the position of the planet relative to the wave. We expect that the interaction with smaller-sized turbulent cells is similar to the observed interaction with MHD waves, but that the duration of the interaction is shorter. As a result of such interactions, a torque is exerted on the planet during short intervals of time, and the planet's semimajor axis varies stochastically under the action of these torques.

Based on our observations with both the low- and high-amplitude waves we can schematically describe the interaction between a planet and a turbulent cell (see Fig. 12). When the planet is at the outer edge of the cell (the side that is farther from the star), the density is increasing toward the planet ($n > 0$), and so we expect the torque to be negative and the planet to migrate inward. Conversely, when the planet is on the inner edge of the cell (the side that is closer to the star), the density decreases toward the star ($n < 0$), and so we expect the torque to be positive and the planet to migrate outward. This inward-outward migration does not “trap” the planet, because the cell is moving away from the star, so this is a transient process.

9 CONCLUSIONS

We investigated the migration of a low-mass planet ($5M_{\oplus}$) in magnetized discs using a Godunov-type HLLD MHD code

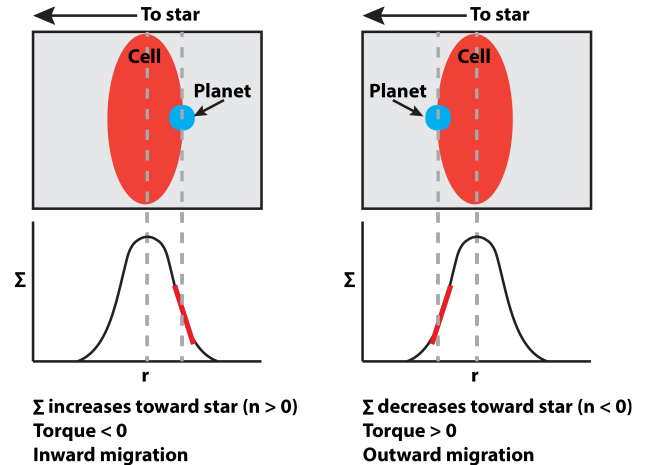


Figure 12. Schematic showing the interaction between a planet and a turbulent cell.

in polar coordinates (Koldoba et al. 2015). The initial surface magnetic field is azimuthal, with different radial distributions $B_{\phi} \sim r^{-k}$, and different strengths determined by the initial plasma parameter at the planet's location, β_i , which varied between $\beta_i = 1$ and 100. We also varied the initial radial surface density distribution in the disc, $\Sigma \sim r^{-n}$. Our main conclusions are as follows:

- (i) In strongly-magnetized discs ($\beta_i = 1, 2$), and where the

density distribution in the disc is flat ($n = 0$), the planet's migration is strongly influenced by magnetic resonances, which are excited near the planet and exert a positive torque on the planet. The migration slows down when the magnetic field distribution is flat ($k = 0$); it slows down more strongly when the magnetic field increases towards the star ($k = 1$); and the migration reverses when the field steeply increases towards the star ($k = 2$). These results are in accord with theoretical predictions by Terquem (2003) and simulations by Fromang et al. (2005).

(ii) Compared with Fromang et al. (2005), we investigated the effect of magnetic resonances on the migration of a planet in discs with different density distributions. We observed that the steepness of the density distribution strongly influences the rate and direction of the migration. When the density increases towards the star ($n = 1$) the planet migrates inward at any steepness of the magnetic field ($k = 0, 1, 2$) and the effect of the magnetic resonances is negligibly small. This is because, at larger density steepness, the negative differential Lindblad torque is much larger than the positive corotation or magnetic torques. In the opposite situation, when the density in the disc decreases toward the star ($n = -0.5$), and the positive corotation torque almost balances the negative Lindblad torque, the role of the positive magnetic torque becomes very significant. The planet migrates outward due to magnetic resonances at all values of the magnetic field steepness ($k = 0, 1, 2$).

(iii) Experiments with a larger mass planet, $20M_{\oplus}$, show that the action of the magnetic resonances is similar to that in the case of a lower-mass planet: the positive torque increases with the steepness of the field, as predicted by the theory. We also observed that, at $k = 2$, the more massive planet migrates outward more rapidly than the lower-mass planet. This is in accord with Eqn. (65) of Terquem (2003), in which the migration time scale is shown to be $\propto M_p^{-1}$.

(iv) We investigated weakly-magnetized discs with initial plasma parameter $\beta_i = 10 - 100$. We observed that non-axisymmetric motions in the disc lead to the formation of a radial component of the magnetic field, its stretching by the differential rotation in the disc, and subsequent MRI-driven turbulence in the disc. Interaction between the planet and turbulent cells leads to stochastic migration, similar to that observed in 3D discs by, e.g., Nelson & Papaloizou (2004). We investigated the transition from the laminar to turbulent disc that often starts near vicinity of the planet, where non-axisymmetric density waves are excited by the planet. The turbulence starts more rapidly when the planet is more massive.

(v) The torques acting on the planet are larger in turbulent discs than in the laminar discs, leading to more rapid migration. However, the direction of the migration is also stochastic, and outward migration is frequently observed.

(vi) To understand how planets interact with individual turbulent cells, we investigated the propagation of a planet through density waves in the disc. We observed that a planet experiences a strong negative torque when it is located inside the wave or at the outer edge of the wave (where the density increases towards the star). However, when the planet is located at the inner edge of the wave (where the density decreases towards the star), then it experiences a positive corotation torque, and it migrates away from the star. We conclude

that the stochastic motion of the planet is connected with the alternating action of these positive and negative torques.

ACKNOWLEDGMENTS

We gratefully acknowledge support from the NASA Research Opportunities in Space and Earth Sciences (ROSES) Origins of Solar Systems grant NNX12AI85G. We also acknowledge support from grants FAP-14.B37.21.0915, SS-1434.2012.2, and RFBR 12-01-00606-a. AVK was supported by the Russian academic excellence project “5top100”. Resources supporting this work were provided by the NASA High-End Computing (HEC) Program through the NASA Advanced Supercomputing (NAS) Division at the NASA Ames Research Center and the NASA Center for Computational Sciences (NCCS) at Goddard Space Flight Center.

REFERENCES

- Armitage P.J. & Rice W.K.M. 2006 in A Decade of Extrasolar Planets around Normal Stars: Proceedings of the Space Telescope Science Institute Symposium held in Baltimore, Maryland, May 2-5, 2005, ed. M. Livio, K. Sahu, & J. Valenti (Baltimore: STScI)
- Balbus S.A., & Hawley J.F. 1991, *ApJ*, 376, 214
- Balbus S.A. & Hawley J.F. 1998, *Rev. Mod. Phys.*, 70, 1
- Lovelace R. V. E., Romanova M. M., Barnard A. W. 2008, *MNRAS*, 389, 1233
- Baruteau C., Fromang S., Nelson R. P., Masset F. 2011, *A&A*, 533, A84
- Baruteau C. & Masset F. 2008, *ApJ*, 672, 1054
- Fromang S., Terquem C., Nelson R.P. 2005, *MNRAS*, 363, 943
- Fu W. & Lai D. 2011, *MNRAS*, 410, 399
- Goldreich P., Tremaine S. 1979, *ApJ*, 233, 857
- Hawley J. F. 2000, *ApJ*, 528, 462
- Hoyle F. & Ireland J.G. 1960, *MNRAS*, 120, 173
- Guilet J., Baruteau C., Papaloizou J. C. B. 2013, *MNRAS*, 430, 1764
- Kley W., Bitsch B., Klahr H. 2009, *A&A*, 506, 971
- Kley W. & Nelson R.P. 2012, *Ann. Rev. Astron. Astrophys.*, 50, 211
- Koldova A.V., Ustyugova G.V., Lii P.S., Comins M.L., Dyda S., Romanova M.M., Lovelace R.V.E. 2015, *New Astronomy*, submitted
- Masset F. S. 2001, *ApJ*, 558, 453
- Masset F. S. 2002, *A&A*, 387, 605
- Masset F. S., Morbidelli A., Crida A., Ferreira J. 2006, *ApJ*, 642, 478
- Masset F. S. & Casoli J. 2009, *ApJ*, 703, 857
- Masset F. S. & Casoli J. 2010, *ApJ*, 723, 1393
- Meyer-Vernet N. & Sicaudy B. 1987, *Icarus*, 69, 157
- Murray C. D. & Dermott S. F. 1999, *Solar System Dynamics*, Cambridge University Press, Cambridge
- Nelson R. P., Papaloizou J. C. B. 2004, *MNRAS*, 350, 849
- Paardekooper S. -J., Baruteau C., Crida A., Kley W. 2010, *MNRAS*, 401, 1950
- Paardekooper S. -J., Baruteau C., Kley W. 2011, *MNRAS*, 410, 293
- Paardekooper S. -J. & Mellema G. 2006, *A&A*, 459, L17

- Paardekooper S. -J. & Papaloizou J. C. B. 2008, A&A, 485, 877
Parker E.N. 1966, ApJ, 145, 811
Shakura N. I. & Sunyaev R. A. 1973, A&A, 24, 337
Shu F. -H. 1984, Planetary Rings, Univ. of Arizona Press, Tucson
Tanaka H., Takeuchi T., Ward W. R. 2002, ApJ, 565, 1257
Terquem C.E.J.M.L.J. 2003, MNRAS, 341, 1157
Terquem C., & Papaloizou J.C.B. 1996, MNRAS, 279, 767
Uribe A. L., Klahr H., Flock M., Henning Th. 2011, ApJ, 736, 85
Ward W. R. 1986, Icarus, 67,164
Ward W. R. 1997, Icarus, 126, 261